RSC Advances

PAPER

View Article Online
View Journal | View Issue

Cite this: *RSC Adv.*, 2022, **12**, 18144

Effect of tertiary amino groups in the hydrophobic segment of an amphiphilic block copolymer on zinc phthalocyanine encapsulation and photodynamic activity†

Makoto Obata, *[a] Eika Ishihara[a] and Shiho Hirohara[b]

Polymer micelles are promising nanocarriers for hydrophobic photosensitizers of photodynamic therapy (PDT). Poly(styrene-*co*-(2-(*N*,*N*-dimethylamino)ethyl acrylate))-*block*-poly(polyethylene glycol monomethyl ether acrylate) (P(St-*co*-DMAEA)-*b*-PPEGA; **1**) was prepared *via* reversible addition and fragmentation chain transfer (RAFT) polymerization as a carrier for a zinc phthalocyanine (ZnPc) photosensitizer to be used in PDT. The DMAEA-unit composition in the P(St-*co*-DMAEA) segment was adjusted to 0.40 molar ratio, which caused a sharp increase in water-solubility when the pH decreased from 7.4 to 5.0. The polymer **1** micelle size distribution also shifted to lower when the pH decreased, whereas this change was not observed in PSt-*co*-PPEGA (**2**), which was previously reported. The UV-vis spectrum of the ZnPc-loaded micelles of polymer **1** exhibited relatively sharp Q bands, comparable to those measured in DMSO, indicating good compatibility of the condensed core with ZnPc. ZnPc-loaded micelles of polymer **1** exerted excellent photocytotoxicity in the MNNG-induced mutant of the rat murine RGM-1 gastric epithelial cell line (RGK-1). In contrast, the ZnPc-loaded micelles of polymer **2** were completely inactive under the same conditions. Fluorescence from the RGK-1 cells treated with ZnPc-loaded micelles of polymer **1** was observed after 4 h of co-incubation, while no fluorescence was observed in cells treated with ZnPc-loaded micelles of polymer **2**. These results indicate that the pH-responsive nature and good compatibility with ZnPc exhibited by the polymer **1** micelles are essential characteristics of ZnPc carriers for efficient photodynamic therapy.

Received 6th April 2022
Accepted 14th June 2022

DOI: 10.1039/d2ra02224a

rsc.li/rsc-advances

Introduction

Photodynamic therapy (PDT) is a minimally-invasive cancer therapy using photosensitizers and light that is currently applied to esophageal cancer and non-small cell lung cancer.[1–8] After a photosensitizer is administered to a patient and accumulates at the tumor site, photoirradiation is used to generate a cytotoxic reactive oxygen species (ROS). Several mechanisms have been suggested to kill tumor cells, such as initiating the apoptosis cascade and vascular shutdown. In addition to being precisely controlled by photoirradiation, tumor-accumulating photosensitizers regulate legions to eliminate malignancies. Limited light availability in the deeper tissue is a major drawback in PDT treatment. Effective photosensitizers must absorb light in the near-infrared (NIR) region,[9–11] due to the fact that longer wavelength increases tissue transparency.

Zinc phthalocyanine (ZnPc) derivatives have many advantages such as high absorption ability in the first near-infrared (NIR-I) window, good ROS-generation efficiency, and excellent photostability.[12–14] However, ZnPc derivatives are highly hydrophobic and tend to aggregate which decreases their photosensitizing ability. Therefore, many attempts have been made to increase the water solubility of phthalocyanine derivatives. The most straightforward approach is the conjugation of hydrophilic elements such as sulfo,[15–19] carboxyl,[19–21] amino,[22] ammonio,[20,23–26] hydroxy,[27] guanidyl,[28,29] and morpholine groups,[30] as well as polyethylene glycol moieties[31–37] at peripheral and non-peripheral positions. This strategy also affords additional functionalities such as tumor-targeting ligands, including carbohydrates[38–42] and peptides.[43–48] However, this approach frequently requires laborious synthetic work, and the resulting photosensitizers are very costly.

Another promising approach is the use of drug delivery system (DDS) technology. This allows us to design the photosensitizer and carrier separately to meet photophysical and physiological requirements, respectively. Among the many types of carriers for PDT photosensitizers, polymer micelles are

[a]*Graduate Faculty of Interdisciplinary Research, University of Yamanashi, 4-4-37 Takeda, Kofu 400-8510, Japan. E-mail: mobata@yamanashi.ac.jp; Fax: +81 55 220 8549; Tel: +81 55 220 8549*

[b]*Department of Chemical and Biological Engineering, National Institute of Technology, Ube College, 2-14-1 Tokiwadai, Ube 755-8555, Japan*

† Electronic supplementary information (ESI) available. See https://doi.org/10.1039/d2ra02224a

very promising nanomaterials because of their biocompatibility and synthetic availability. Several ZnPc-loaded polymer micelles have been prepared using amphiphilic block copolymers such as poly(ethylene glycol)-*b*-poly(L-lactide) (PEG-*b*-PLLA),[49–51] poly(ethylene glycol)-*b*-poly(ε-caprolacton) (PEG-*b*-PCL),[52] and more highly sophisticated polymers.[53–55] ZnPc can be physically trapped in the hydrophobic core of the polymer micelle. However, most ZnPc-loaded polymer micelles show severely broadened UV-vis spectra, indicating the formation of ZnPc aggregates. Aggregation changes the photophysical properties of ZnPc molecules, and deactivates the photodynamic effect.[56,57] Previously, we demonstrated the synthesis of polystyrene-*b*-poly(polyethylene glycol monomethyl ether acrylate) (PSt-*b*-PPEGA) and the preparation of ZnPc-loaded polymer micelles.[58] The efficiency of encapsulating ZnPc depended on the molecular architecture of PSt-*b*-PPEGA. Disappointingly, the photocytotoxicity of the resulting ZnPc-loaded polymer micelles was very low in HeLa cells. Similar to their behavior in other polymer micelles, ZnPc molecules are strongly aggregated in the polymer micelles, as evidenced by the UV-vis spectra. In addition, the ZnPc-loaded polymer micelles were kinetically frozen and lacked the ability to release ZnPc. Hence, the ZnPc molecules trapped in the polymer micelles were photochemically inactivated. This might have caused the low photocytotoxicity of ZnPc-loaded polymer micelles. Therefore to achieve successful PDT treatment, it is crucial that carriers physically encapsulate ZnPc and prevent its aggregation.

Recently, Borovkov *et al.* reported that a mixture of a π-accepting solvent such as chlorobenzene and a nitrogenous base such as triethylamine dissolves ZnPc to make a clear solution with molecular dispersion.[59] In addition, we demonstrated that the side group of the hydrophobic chain affects the aggregating behavior of ZnPc in the polymer micelles.[60] These two findings inspired us to investigate the molecular dispersion of ZnPc in polymer micelles with the hydrophobic chains consisting of repeating units with aromatic rings and tertiary amines. In addition, tertiary amines, with pK_a values approximately 6.5–7.0, can be used as a pH-sensitive element between the extracellular physiological environment (pH = 7.4) and acidic organelles (pH = 5.0) during cellular internalization. In this study, we synthesized a pH-responsive amphiphilic block copolymer using 2-(*N*,*N*-dimethylamino)ethyl acrylate (DMAEA) as a pH-sensitive element, and preparation of the ZnPc-loaded polymer micelles. The pH-responsive properties, aggregating behavior of ZnPc, and photocytotoxicity of the polymer micelles are discussed.

Results and discussion

Design of pH-responsive hydrophobic chain

To provide a pH-response ability, we designed a copolymer of styrene and DMAEA as a hydrophobic segment. First, an appropriate molar fraction of DMAEA units in the copolymer,

Table 1 Synthesis of P(St-*co*-DMAEA) for solubility test *via* RAFT polymerization[a]

Run no.	f_{DMAEA}[b]	Yield[c] (%)	F_{DMAEA}[d]	M_n (M_w/M_n)[e]
1	0.10	15	0.12	10 500 (1.07)
2	0.20	14	0.21	9900 (1.08)
3	0.30	20	0.29	13 600 (1.09)
4	0.40	8	0.36	10 200 (1.14)
5	0.60	21	0.48	8300 (1.40)
6	0.80	22	0.64	6200 (1.55)

[a] Bulk polymerization; $[St + DMAEA]_0/[CPADB]_0/[AIBN]_0 = 500/1/0.2$; polym. temp., 60 °C; polym. time, 24 h. [b] Mole fraction of DMAEA in the feed. [c] Isolated yield. [d] Mole fraction of DMAEA unit in the copolymer. [e] Number average molecular mass and dispersity determined by SEC using polystyrene standards.

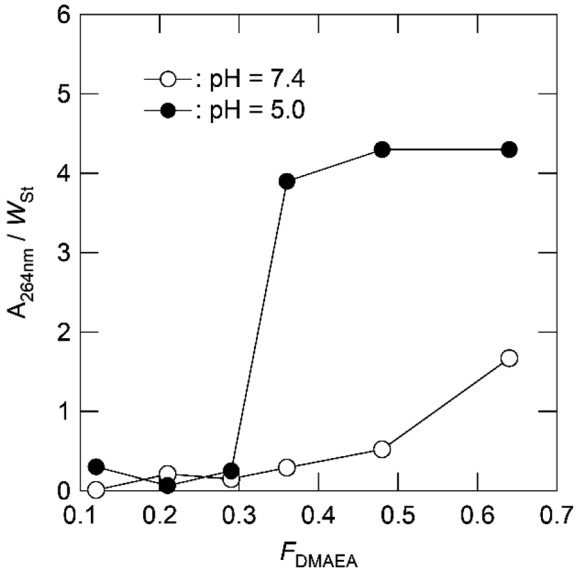

Fig. 1 Relative solubility of P(St-*co*-DMAEA) in PBS (pH = 7.4; open circle) and in PBS adjusted to a pH of 5.0 by adding HCl (filled circle) as a function of the F_{DMAEA} value.

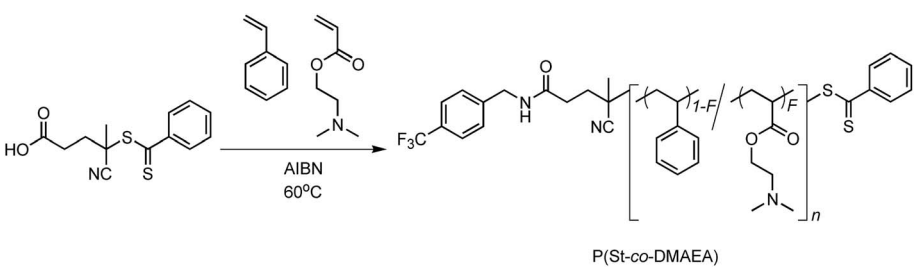

Scheme 1 Synthesis of P(St-*co*-DMAEA) for solubility test *via* RAFT polymerization.

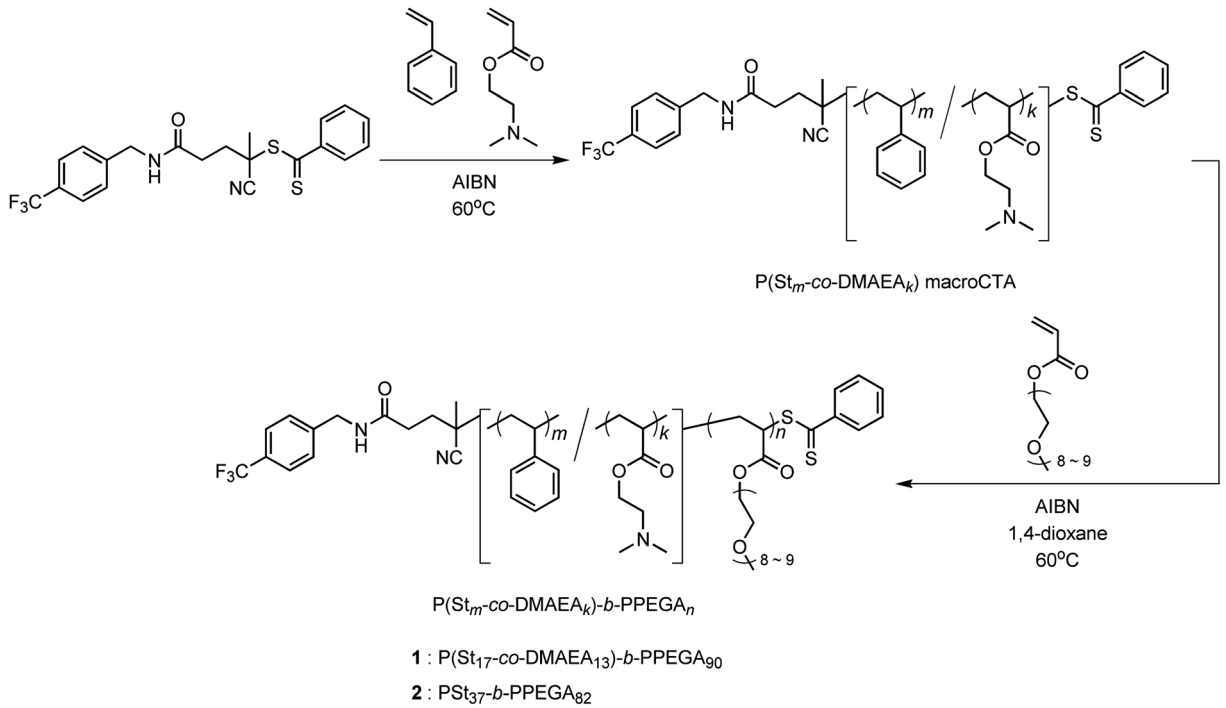

Scheme 2 Synthesis of P(St$_{17}$-*co*-DMAEA$_{13}$)-*b*-PPEGA$_{90}$ (**1**) and PSt$_{37}$-*b*-PPEGA$_{82}$ (**2**) *via* RAFT polymerization.

Table 2 Synthesis of P(St$_m$-*co*-DMAEA$_k$) macroCTA *via* RAFT polymerization[a]

Run no.	f_{DMAEA}[b]	x_{St}[c]	x_{DMAEA}[c]	Yield[d] (%)	k[e]	m[e]	$M_{n,NMR}$[f]	M_n (M_w/M_n)[g]
1	0.40	0.29	0.13	7	16	12	3400	2800 (1.10)
2	0	0.27	—	12	37	0	4300	3700 (1.08)

[a] Bulk polymerization; [St + DMAEA]$_0$/[CF$_3$-CPADB]$_0$/[AIBN]$_0$ = 200/1/0.1; polym. temp., 60 °C; polym. time, 24 h. [b] Mole fraction of DMAEA in the feed. [c] Conversions of St (x_{St}) and DMAEA (x_{DMAEA}) determined by ^{1}H NMR spectroscopy. [d] Isolated yield. [e] Number average degree of polymerization of St (m) and DMAEA (k) determined by ^{1}H and ^{19}F NMR spectroscopies using cross reference. [f] Number average molecular mass calculated using the k and m values considering the mass of CF$_3$-CPADB. [g] Number average molecular mass and dispersity determined by SEC using polystyrene standards.

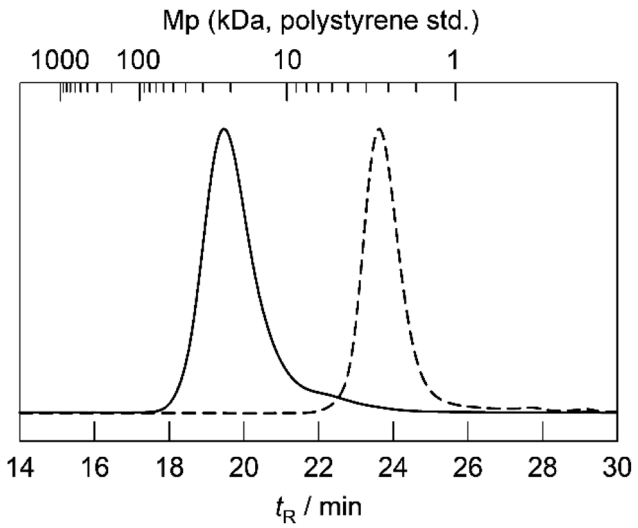

Fig. 2 SEC traces of P(St$_{16}$-*co*-DMAEA$_{12}$) macroCTA (broken line) and polymer **1** (solid line).

P(St-*co*-DMAEA), was investigated to exhibit a large solubility change during the pH shift from 7.4 to 5.0. Six copolymers were prepared by bulk RAFT polymerization using 4-cyano-4-(thiobenzoyl)thiopentanoic acid (CPADB) as a chain transfer agent, as shown in Scheme 1.

The mole fractions of the DMAEA units (F_{DMAEA}), number average molecular mass (M_n), and dispersity (M_w/M_n) of the resulting copolymers are listed in Table 1. The F_{DMAEA} values varied from 0.12 to 0.64, while the M_n values were relatively constant at approximately 10^4, except for the case of F_{DMAEA} = 0.64. The relative water solubility was examined in phosphate-buffered saline (PBS), and PBS adjusted to pH 5.0, by adding HCl. The amount of the copolymer dissolved in the buffered solution was quantified by the absorbance at 264 nm and divided by the weight fraction of styrene units to determine the water solubility of the copolymer. Fig. 1 shows the plots of the relative water solubility as a function of the F_{DMAEA} value of the copolymer. The relative water solubility gradually increased with an increase in the F_{DMAEA} value at pH 7.4. In contrast, the

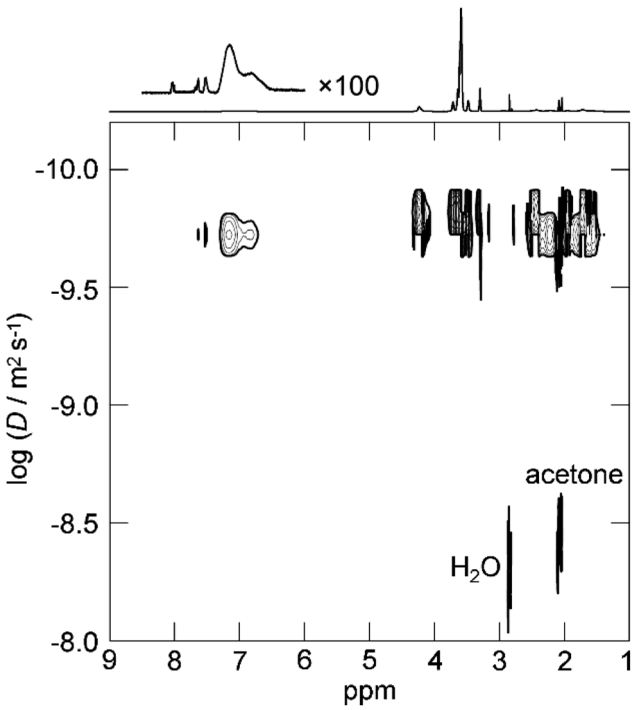

Fig. 3 ^{1}H DOSY spectrum of polymer **1** in acetone-d_6 at 298 K.

relative water solubility suddenly increased at an F_{DMAEA} of approximately 0.3 at pH 5.0. This suggests that the copolymer F_{DMAEA} of approximately 0.3 exerts a large water-solubility change between the physiological environment (pH = 7.4) and acidic intracellular organelles such as endosomes and lysosomes (pH = 5.0). Therefore, we choose the F_{DMAEA} value of 0.4 for the hydrophobic P(St-*co*-DMAEA) segment for the pH-responsive amphiphilic block copolymer.

Synthesis of P(St-*co*-DMAEA)-*b*-PPEGA

The amphiphilic block copolymer, P(St-*co*-DMAEA)-*b*-PPEGA, was synthesized by RAFT polymerization of styrene with

Table 3 Synthesis of P(St_{17}-*co*-$DMAEA_{13}$)-*b*-$PPEGA_{90}$ (**1**) and PSt_{37}-*b*-$PPEGA_{82}$ (**2**) *via* chain extension with PEGA[a]

Symble	x_{PEGA}[b]	Yield[c] (%)	m[d]	k[d]	n[d]	$M_{n,NMR}$[e]	M_n (M_w/M_n)[f]
1	0.49	43	17	13	90	47 400	16 000 (1.25)
2	0.68	57	37	0	82	44 000	15 000 (1.21)

[a] $[PEGA]_0/[P(St_k\text{-}co\text{-}DMAEA_m)\ macroCTA]_0/[AIBN]_0$ = 100/1/0.2; polym. solv., 1,4-dioxane; polym. temp., 60 °C; polym. time, 24 h. [b] Conversion of PEGA (x_{PEGA}) determined by ^{1}H NMR spectroscopy. [c] Isolated yield. [d] Number average degree of polymerization of St (m), DMAEA (k) and PEGA (n) determined by ^{1}H and ^{19}F NMR spectroscopies using cross reference. [e] Number average molecular mass calculated using the k, m and n values considering the mass of CF_3-CPADB. [f] Number average molecular mass and dispersity determined by SEC using polystyrene standards.

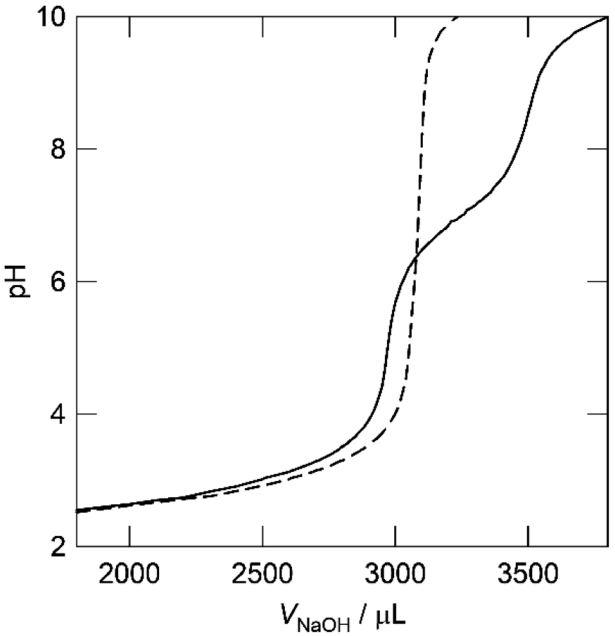

Fig. 5 pH titration curves of polymers **1** (solid line) and **2** (broken line).

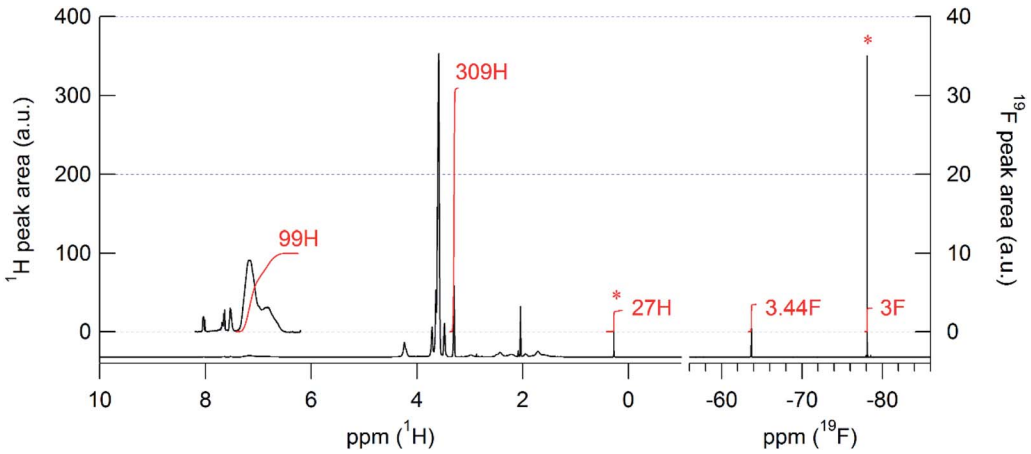

Fig. 4 ^{1}H (left panel) and ^{19}F NMR spectra (right panel) of **1** in acetone-d_6. The asterisks indicate the peaks from CF_3CH_2OTTMS as an internal cross reference for peak area normalization between the ^{1}H and ^{19}F NMR spectra.

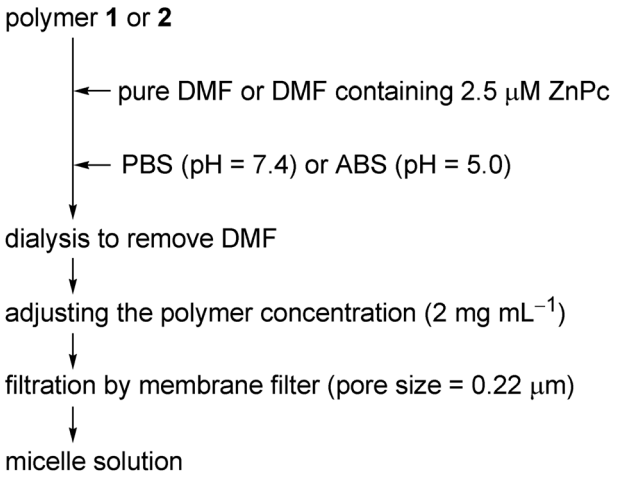

Chart 1 Flow chart for preparation of polymer micelle solution.

DMAEA, followed by chain extension with PEGA, as shown in Scheme 2.

It should be noted that we used trifluoromethyl-labeled CPADB (CF_3-CPADB) as a chain transfer agent to determine the degree of polymerization (DP_n) of each repeating unit by the combination of ^1H and ^{19}F NMR spectroscopies. First, a statistical copolymer, P(St-*co*-DMAEA) macroCTA, was synthesized by bulk RAFT polymerization of styrene with DMAEA using CF_3-CPADB and azobisisobutyronitrile (AIBN) as a chain transfer agent and initiator, respectively, at 60 °C for 24 h. The DP_n values of styrene and DMAEA of the resulting polymer were 16 and 12, respectively, indicating the F_{DMAEA} value was 0.43 (Table 2).

For comparison, a homopolymer, PSt macroCTA, was also synthesized by a similar procedure. The resulting macroCTA was extended with PEGA using AIBN as an initiator in 1,4-dioxane at 60 °C for 24 h to produce block copolymer P(St-*co*-DMAEA)-*b*-PPEGA and PSt-*b*-PPEGA. Fig. 2 shows the SEC traces of P(St-*co*-DMAEA) macroCTA and P(St-*co*-DMAEA)-*b*-PPEGA. The SEC trace of P(St-*co*-DMAEA)-*b*-PPEGA clearly shifted toward a higher molecular mass than that of P(St-*co*-DMAEA) macroCTA without significant broadening.

Fig. 3 shows the ^1H DOSY spectrum of P(St-*co*-DMAEA)-*b*-PPEGA, in which the styrene units exhibit a diffusion coefficient identical to that of the PEGA units. These results indicate the formation of a block copolymer, P(St-*co*-DMAEA)-*b*-PPEGA.

Fig. 4 shows the ^1H and ^{19}F NMR spectra of P(St-*co*-DMAEA)-*b*-PPEGA in acetone-d_6 mixed with tris(trimethylsilyl)-2,2,2-trifluoroethoxysilane (CF_3CH_2OTTMS) as an internal cross-reference for peak area normalization between these two spectra. The trifluoromethyl group at the initiating end was unequivocally identified in the ^{19}F NMR spectrum owing to the nuclear specificity of NMR spectroscopy. The ^{19}F NMR spectrum affords the ratio of polymer to CF_3CH_2OTTMS, while the ^1H NMR spectrum affords the ratio of each repeating unit to CF_3CH_2OTTMS. Therefore, the combination of these two spectra afforded DP_n values for each repeating unit. This ^1H–^{19}F cross-reference technique is helpful for determining the DP_n and M_n values by end group analysis, especially in the case that the polymer affords very intense peaks in the ^1H NMR spectrum, such as a PPEGA segment.

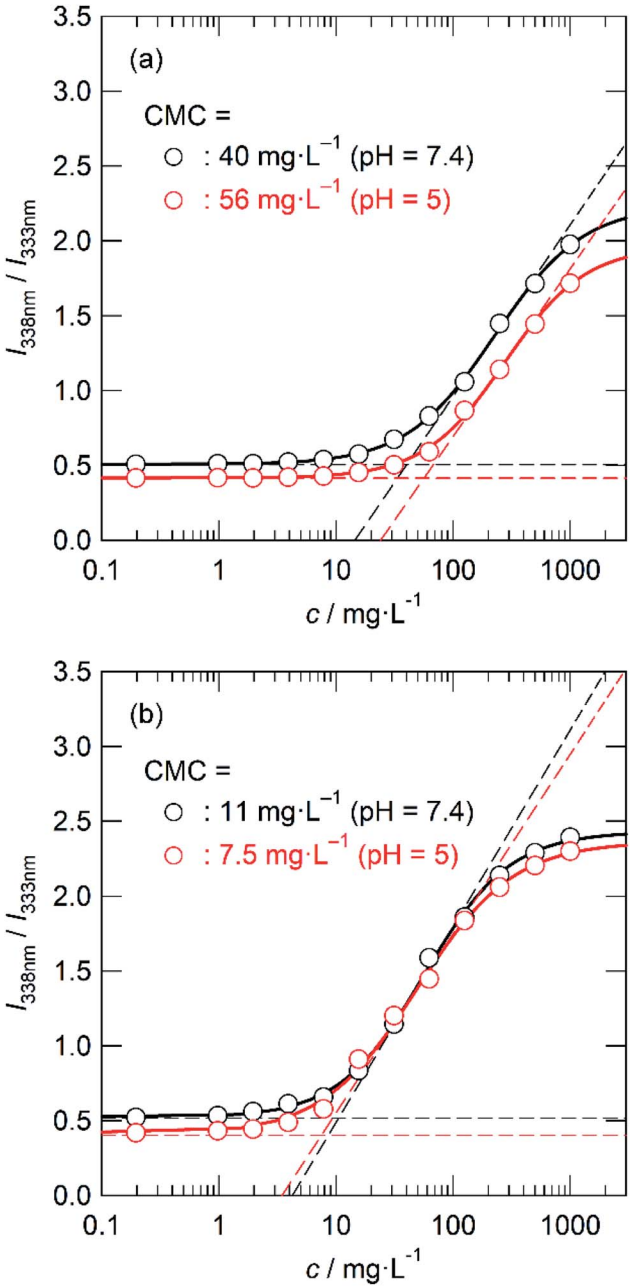

Fig. 6 I_{338}/I_{333} values as a function of the concentration of polymers **1** (a) and **2** (b) in PBS (black, pH = 7.4) and ABS (red, pH = 5). [Pyrene] = 1 mM.

Table 3 summarizes the DP_n values for each repeating unit of the block copolymers. Finally, we obtained a pH-responsive block copolymer, P(St_{17}-*co*-$DMAEA_{13}$)-*b*-$PPEGA_{90}$ (hereinafter denoted as **1**), and the block copolymer, PSt_{37}-*b*-$PPEGA_{82}$ (hereinafter denoted as **2**), as shown in Scheme 2. The pH-responsive nature of the resulting block copolymer was examined by acid–base titration. Fig. 5 shows the titration curves of polymers **1** and **2**. The curve for polymer **1** had an

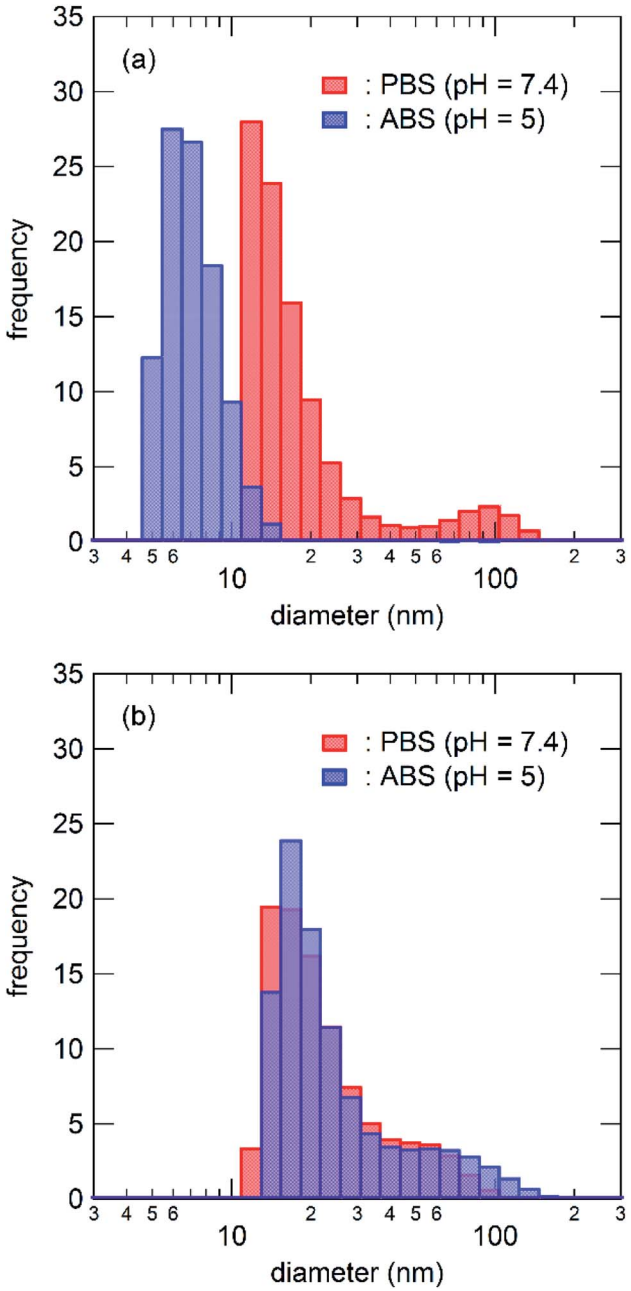

Fig. 7 Size distribution of polymer **1** micelle (a) and polymer **2** micelle (b) in PBS (red, pH = 7.4) and ABS (blue, pH = 5). The polymer concentration was 1000 mg L^{-1}.

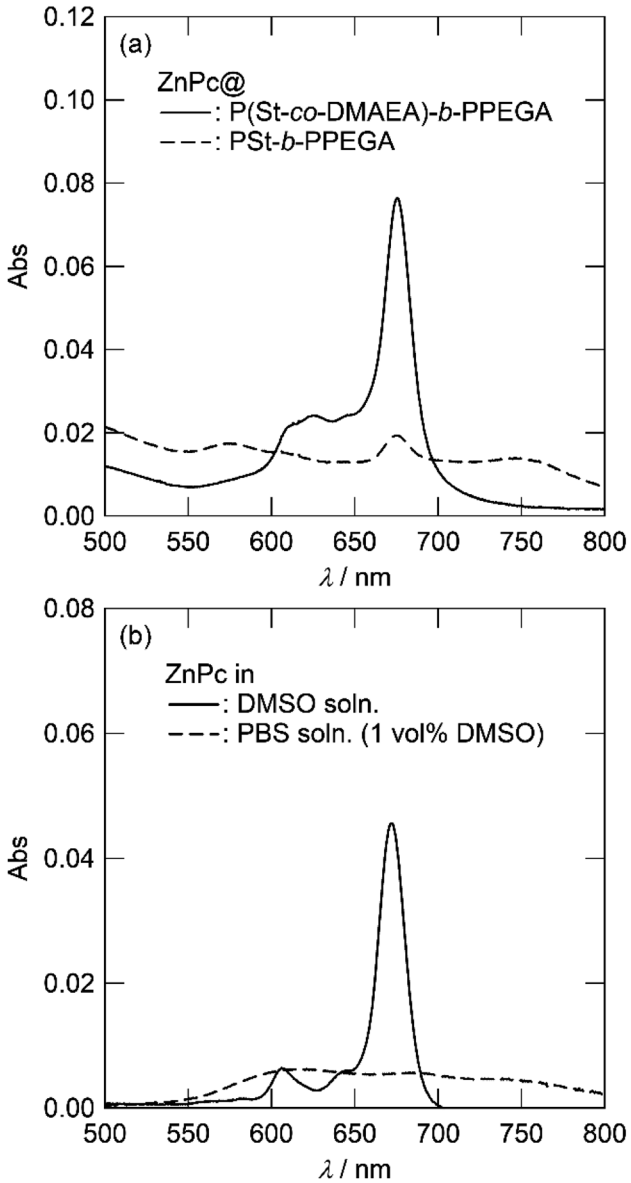

Fig. 8 UV-vis spectra of ZnPc-loaded micelles of polymers **1** ([ZnPc] = 0.52 μM; solid line) and **2** ([ZnPc] = 0.44 μM) in PBS (a) and ZnPc in DMSO and PBS containing 1% DMSO ([ZnPc] = 0.5 μM; b).

inflection point at pH of approximate 7 due to the buffering capacity of DMAEA units, while polymer **2** showed no buffering nature.

Preparation and characterization of polymer micelles

Polymer micelles were prepared by the dialysis method (Chart 1).

Briefly, polymer **1** or **2** was dissolved in DMF and slowly added to the same amount of PBS, then DMF was removed by dialysis to afford a clear solution without any precipitates. After adjusting the polymer concentration to 2 mg mL^{-1}, the solution was filtered through a membrane filter (pore size of 0.22 μm). The critical micelle concentration (CMC) in PBS (pH = 7.4) and acetate buffered saline (ABS, pH = 5.0) was estimated by the fluorometric method using pyrene as a hydrophobic fluorescent probe. Fig. 6 shows plots of the fluorescence intensity ratio (I_{338}/I_{333}) as a function of the logarithm of the polymer concentration.

Interestingly, the plots of polymer **1** in ABS slightly shifted toward higher concentrations than those measured in PBS, while no such shift was observed for polymer **2**. The CMC value was determined by the crossing point of the baseline and the tangent at the inflection point of the best-fitted sigmoidal curve. The CMC value of polymer **1** was determined to be 40 mg L^{-1} in PBS and changed to 56 mg L^{-1} in ABS. Significant changes due

to the pH switch were also observed in dynamic light scattering (DLS) measurements. Fig. 7 shows the size distribution of the micelles of polymers **1** and **2** in PBS and ABS at a polymer concentration of 1 mg mL^{-1}. The size distribution of the micelles of polymer **1** shifted to lower when the pH changed from 7.4 to 5.0. In contrast, no changes were observed for polymer **2**. These results suggest that DMAEA units act as pH-responsive moieties to destabilize the polymeric micelles under acidic conditions.

Zinc phthalocyanine (ZnPc), a highly hydrophobic photosensitizer, was used as the payload of these polymer micelles. ZnPc-loaded micelles were prepared by a procedure similar to that of free micelles except for the use of a DMF solution of ZnPc instead of pure DMF. After dialysis and adjustment of the polymer concentration, insoluble ZnPc precipitates were removed by filtration with a membrane filter (pore size 0.22 μm). The concentrations of ZnPc in the micelle solutions were determined spectrofluorometrically and are listed in Table 4.

Triplicate experiments suggest that the encapsulation efficiency (E.E.) did not depend on the presence of DMAEA units, and ranged from 28% to 73%. Fig. 8 shows the UV-vis spectra of ZnPc-loaded polymer micelles in PBS. The ZnPc-loaded micelles of polymer **2** showed a broadened absorption band, indicating that ZnPc molecules were tightly aggregated in the hydrophobic core. In contrast, the ZnPc-loaded micelles of polymer **1** showed Q bands similar to those recorded in dimethyl sulfoxide (DMSO). Therefore, the micelles of polymer **1** afford the microenvironment to dissolve ZnPc in a monomeric form. The difference in the microenvironment of the polymer micelles crucially affects the photophysical and photodynamic effects of ZnPc.

In vitro photocytotoxicity of ZnPc-loaded polymer micelles

The *in vitro* photocytotoxicity of ZnPc-loaded micelles was examined in MNNG-induced mutant of the rat murine RGM-1 gastric epithelial cell line (RGK-1).[61] RGK-1 cells were co-incubated with the micelles in a mixture of PBS and culture medium (1/1, v/v) for 24 h. After removing the excess amount of the drug, the cells were photoirradiated with a 100 W halogen lamp equipped with a Y-50 cut filter. The cell survival rate was determined by WST-8 assay and normalized by the value for no drug treatment with photoirradiation. Fig. 9a shows the cell survival rate after treatment with the payload-free micelles of polymers **1** and **2** at a concentration of 1 mg mL^{-1} as a function of the light dose. Fig. 9a indicates that the micelles of **1** and **2** essentially have no cytotoxicity regardless of photoirradiation. The cell survival rates after the ZnPc-loaded polymer micelle treatment are shown in Fig. 9b. ZnPc-loaded micelles of **1** and **2** did not show cytotoxicity without photoirradiation (light dose of 0 J cm^{-2}). ZnPc-loaded micelles of **2** did not show cytotoxicity even upon photoirradiation at a light dose of 20 J cm^{-2}. This can be expected because of the very low ZnPc concentration in comparison to that used in our previous study.[58] In contrast, ZnPc-loaded micelles of **1** exerted excellent photocytotoxicity under the same condition; almost complete annihilation was achieved upon photoirradiation of 20 J cm^{-2} with a ZnPc dose of only 0.05 μM.

Fig. 10 shows the images of RGK-1 cells co-incubated with ZnPc-loaded polymer micelles captured by fluorescence microscopy. The red fluorescence from the cells treated with ZnPc-loaded micelles of **1** gradually increased with co-incubation time. In contrast, almost no fluorescence was observed in the cells treated with **2**. This distinct difference in the photophysical behavior in the cellular microenvironment affected the photocytotoxicity of the ZnPc-loaded micelles.

The photodynamic behavior of ZnPc-loaded micelles of **1** and **2** should be related to the fate of polymer micelles co-incubated with cells, that is, cellular uptake *via* endocytosis, endosome escape, and ZnPc release or conservation in polymer micelles. The pH-responsive nature of **1** enhances endosome escape and facilitates ZnPc release. However, another mechanism is also possible. If the polymer micelle is stable enough in the cellular microenvironment, ZnPc encapsulated in the micelles of **1** must be photochemically active rather than that in **2**. The first hypothesis is a line along with the usual drug

Table 4 Preparation of the micelle solutions of polymers **1** and **2**[a]

	In preparation			Micelle solution		
Run no.	Polymer[b]	[ZnPc][c] (μM)	Buffer[d]	[ZnPc][e] (μM)	E.E.[f] (%)	$D_{50\%}$[g] (nm)
1	**1**	0	PBS	0	—	18
2	**1**	0	ABS	0	—	7
3	**2**	0	PBS	0	—	20
4	**2**	0	ABS	0	—	20
5	**1**	2.5	PBS	0.73	73	79
6	**1**	2.5	PBS	0.63	63	n.d.
7	**1**	2.5	PBS	0.52	52	n.d.
8	**2**	2.5	PBS	0.28	28	33
9	**2**	2.5	PBS	0.58	58	n.d.
10	**2**	2.5	PBS	0.44	44	n.d.

[a] [Polymer] = 2 mg mL^{-1}. [b] **1**, P(St_{17}-*co*-$DMAEA_{13}$)-*b*-$PPEGA_{90}$; **2**, PSt_{37}-*b*-$PPEGA_{82}$. [c] Concentration of ZnPc in DMF for dissolving the polymer. [d] PBS, phosphate buffered saline (pH 7.4); ABS, acetate-buffered saline (pH 5.0). [e] Concentration of ZnPc in the micelle solution determined by spectrofluorometry. [f] Encapsulation efficiency defined as E.E. (%) = $([ZnPc]_{micelle} \times 5)/([ZnPc]_{DMF} \times 2) \times 100$. [g] Median diameter, as determined by DLS.

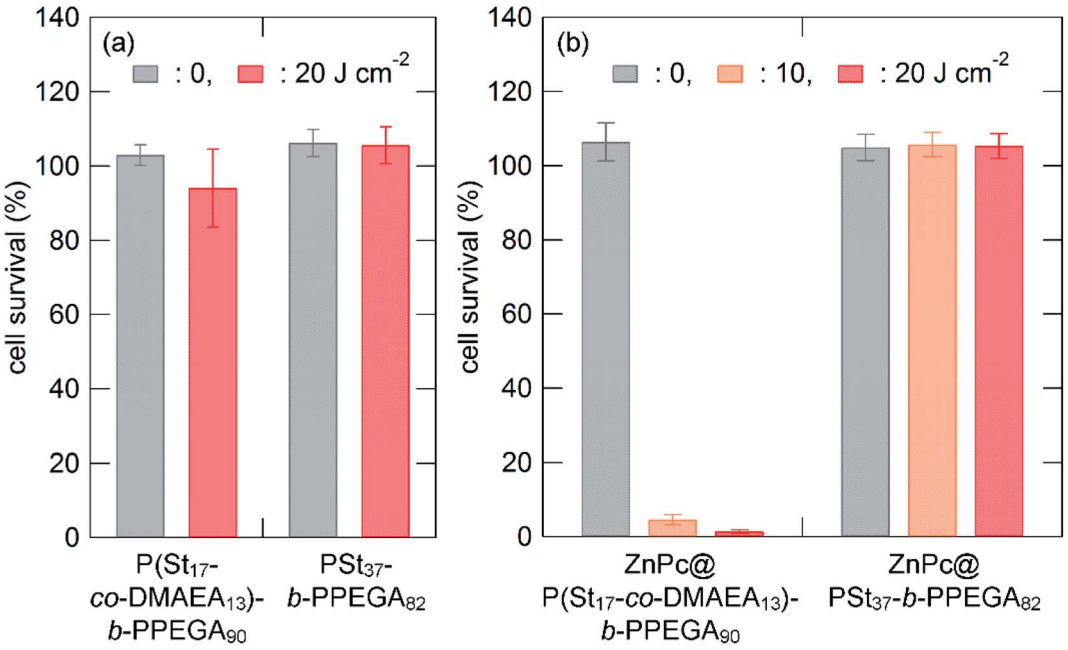

Fig. 9 *In vitro* dark and photocytotoxicity of polymers **1** and **2** (a; [polymer] = 1000 mg L^{-1}) and their ZnPc-loaded micelles of polymers **1** and **2** (b; [ZnPc] = 0.05 μM) in RGK-1 cells as a function of the light dose. The photoirradiation was provided by a 100-W halogen lamp equipped with a Y-50 cutoff filter (λ > 500 nm). The values are the mean ± standard deviation of six replicate experiments.

delivery regime, in which polymer micelles act as simple carriers for photosensitizers. However, the latter hypothesis is beyond the simple drug delivery regime; polymer micelles provide a suitable microenvironment for photosensitizers. The key is the kinetic properties of polymer micelles, which are not yet fully understood, especially in very complicated microenvironments such as the cytosol. To address this issue, a study on the behavior of micelles of **1** is in progress in our laboratory using Förster resonance energy transfer (FRET) and aggregation-induced emission (AIE) dye labeling techniques.

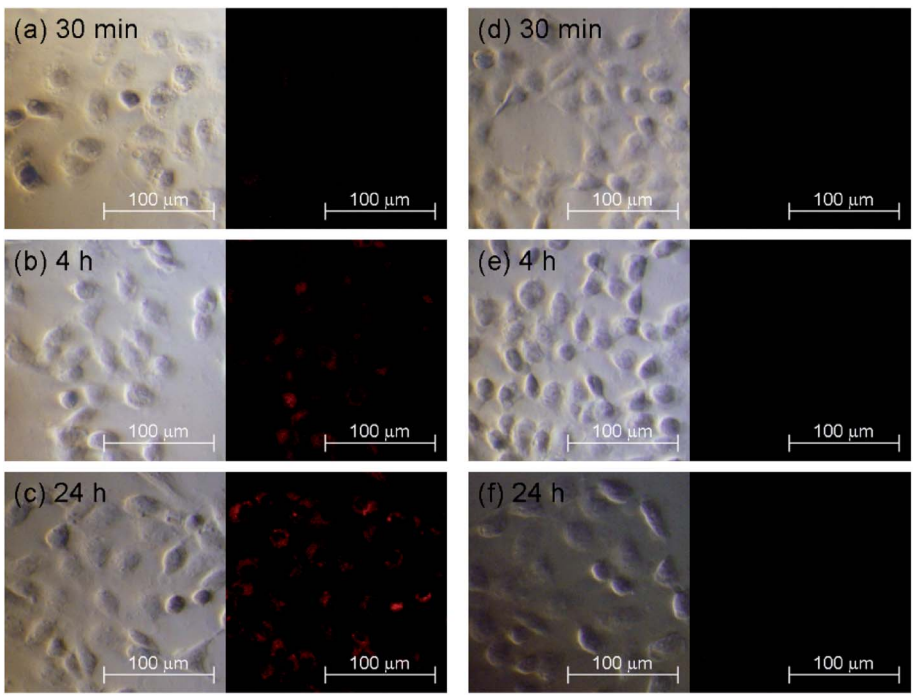

Fig. 10 Bright field (left panel) and fluorescence images (right panel) of RGK-1 cells incubated in the presence of ZnPc-loaded micelles of polymers **1** (a, 30 min; b, 4 h; c, 24 h) and **2** (d, 30 min; e, 4 h; f, 24 h).

Conclusions

Amphiphilic block copolymers, P(St-*co*-DMAEA)-*b*-PPEGA (**1**) and PSt-*b*-PPEGA (**2**), were successfully prepared by successive RAFT polymerizations. The mole fraction of styrene units in P(St-*co*-DMAEA) of **1** was 0.4, which caused the water solubility to increase when the pH decreased from 7.4 to 5.0. Polymers **1** and **2** both formed micelles in PBS. The unique nature of **1** was evidenced by DLS and the UV-vis measurements. DLS results revealed the pH sensitivity of the micelles of **1**: the size distribution of the micelle of **1** dramatically shifted lower with a decrease in the pH, while that of **2** did not change. The UV-vis spectrum of ZnPc-loaded micelles of **1** indicated the excellent compatibility of the core components of the micelle with ZnPc: the Q bands of ZnPc-loaded micelle of **1** were very similar to those observed in DMF, while those of **2** were severely broadened. ZnPc-loaded micelle of **1** exerted excellent photocytotoxicity in RGK-1 cells and showed distinct photochemical behavior in the cellular microenvironment compared to **2**. The enhanced PDT effect of polymer **1** micelles should be related to its pH-responsive nature and good compatibility with ZnPc.

Conflicts of interest

There are no conflicts to declare.

Acknowledgements

The authors wish to thank Prof. Hidenori Okuzaki, University of Yamanashi for support with the DLS measurements. This work was supported by JSPS KAKENHI (grant numbers 21550156, 25410126, and 17K05877).

Notes and references

1 T. C. Pham, V. N. Nguyen, Y. Choi, S. Lee and J. Yoon, *Chem. Rev.*, 2021, **121**, 13454–13619.
2 A. Escudero, C. Carrillo-Carrión, M. C. Castillejos, E. Romero-Ben, C. Rosales-Barrios and N. Khiar, *Mater. Chem. Front.*, 2021, **5**, 3788–3812.
3 S. Wang, X. Wang, L. Yu and M. Sun, *Photodiagn. Photodyn. Ther.*, 2021, **34**, 102254.
4 B. Mansoori, A. Mohammadi, M. A. Doustvandi, F. Mohammadnejad, F. Kamari, M. F. Gjerstorff, B. Baradaran and M. R. Hamblin, *Photodiagn. Photodyn. Ther.*, 2019, **26**, 395–404.
5 M. Lan, S. Zhao, W. Liu, C.-S. Lee, W. Zhang and P. Wang, *Adv. Healthcare Mater.*, 2019, **8**, 1900132.
6 S. Kwiatkowski, B. Knap, D. Przystupski, J. Saczko, E. Kędzierska, K. Knap-Czop, J. Kotlińska, O. Michel, K. Kotowski and J. Kulbacka, *Biomed. Pharmacother.*, 2018, **106**, 1098–1107.
7 S. Yano, S. Hirohara, M. Obata, Y. Hagiya, S. Ogura, A. Ikeda, H. Kataoka, M. Tanaka and T. Joh, *J. Photochem. Photobiol., C*, 2011, **12**, 46–67.
8 J. P. Celli, B. Q. Spring, I. Rizvi, C. L. Evans, K. S. Samkoe, S. Verma, B. W. Pogue and T. Hasan, *Chem. Rev.*, 2010, **110**, 2795–2838.
9 T. L. Rapp and C. A. DeForest, *Adv. Drug Delivery Rev.*, 2021, **171**, 94–107.
10 C. Ash, M. Dubec, K. Donne and T. Bashford, *Laser Med. Sci.*, 2017, **32**, 1909–1918.
11 P. Avci, A. Gupta, M. Sadasivam, D. Vecchio, Z. Pam, N. Pam and M. R. Hamblin, *Semin. Cutaneous Med. Surg.*, 2013, **32**, 41–52.
12 P. C. Lo, M. S. Rodríguez-Morgade, R. K. Pandey, D. K. P. Ng, T. Torres and F. Dumoulin, *Chem. Soc. Rev.*, 2020, **49**, 1041–1056.
13 L. P. Roguin, N. Chiarante, M. C. García Vior and J. Marino, *Int. J. Biochem. Cell Biol.*, 2019, **114**, 105575.
14 C. M. Allen, W. M. Sharman and J. E. Van Lier, *J. Porphyrins Phthalocyanines*, 2001, **5**, 161–169.
15 T. Ikeuchi, J. Mack, T. Nyokong, N. Kobayashi and M. Kimura, *Langmuir*, 2016, **32**, 11980–11985.
16 R. Liang, S. You, L. Ma, C. Li, R. Tian, M. Wei, D. Yan, M. Yin, W. Yang, D. G. Evans and X. Duan, *Chem. Sci.*, 2015, **6**, 5111–5518.
17 N. Cauchon, H. Ali, H. M. Hasséssian and J. E. van Lier, *Photochem. Photobiol. Sci.*, 2010, **9**, 331–341.
18 S. Kudrevich, N. Brasseur, C. La Madeleine, S. Gilbert and J. E. van Lier, *J. Med. Chem.*, 1997, **40**, 3897–3904.
19 J. Griffiths, J. Schofield, M. Wainwright and S. B. Brown, *Dyes Pigm.*, 1997, **33**, 65–78.
20 J. Kollar, M. Machacek, M. Halaskova, J. Lenco, R. Kucera, J. Demuth, M. Rohlickova, K. Hasonova, M. Miletin, V. Novakova and P. Zimcik, *J. Med. Chem.*, 2020, **63**, 7616–7632.
21 H. Yao, K. Xu, J. Zhou, L. Zhou and S. Wei, *ACS Biomater. Sci. Eng.*, 2020, **6**, 450–462.
22 X. Li, X. H. Peng, B. D. Zheng, J. Tang, Y. Zhao, B. Y. Zheng, M. R. Ke and J. D. Huang, *Chem. Sci.*, 2018, **9**, 2098–2104.
23 S. Yan, Q. Huang, X. Song, Z. Chen, M. Huang and J. Zhang, *RSC Adv.*, 2019, **9**, 24560–24567.
24 M. Li, B. Mai, A. Wang, Y. Gao, X. Wang, X. Liu, S. Song, Q. Liu, S. Wei and P. Wang, *RSC Adv.*, 2017, **7**, 40734–40744.
25 M. Machacek, A. Cidlina, V. Novakova, J. Svec, E. Rudolf, M. Miletin, R. Kučera, T. Simunek and P. Zimcik, *J. Med. Chem.*, 2015, **58**, 1736–1749.
26 A. Wang, Y. Li, L. Zhou, L. Yuan, S. Lu, Y. Lin, J. Zhou and S. Wei, *J. Photochem. Photobiol., B*, 2014, **141**, 10–19.
27 M. Hu, N. Brasseur, S. Z. Yildiz, J. E. van Lier and C. C. Leznoff, *J. Med. Chem.*, 1998, **41**, 1789–1802.
28 X. Shi, Q. Zhan, Y. Li, L. Zhou and S. Wei, *Mol. Pharmaceutics*, 2020, **17**, 190–201.
29 B. R. Vummidi, F. Noreen, J. Alzeer, K. Moelling and N. W. Luedtke, *ACS Chem. Biol.*, 2013, **8**, 1737–1746.
30 M. Kucinska, P. Skupin-Mrugalska, W. Szczolko, L. Sobotta, M. Sciepura, E. Tykarska, M. Wierzchowski, A. Teubert, A. Fedoruk-Wyszomirska, E. Wyszko, M. Gdaniec, M. Kaczmarek, T. Goslinski, J. Mielcarek and M. Murias, *J. Med. Chem.*, 2015, **58**, 2240–2255.

31 W. Wang, J. Wang, G. Hong, L. Mao, N. Zhu and T. Liu, *Biomacromolecules*, 2021, **22**, 4284–4294.
32 R. O. Ogbodu, B. Nitzsche, A. Ma, D. Atilla, A. G. Gürek and M. Höpfner, *J. Photochem. Photobiol., B*, 2020, **208**, 111915.
33 W. Kuzyniak, E. A. Ermilov, D. Atilla, A. G. Gürek, B. Nitzsche, K. Derkow, B. Hoffmann, G. Steinemann, V. Ahsen and M. Höpfner, *Photodiagn. Photodyn. Ther.*, 2016, **13**, 148–157.
34 X. Jia, F. F. Yang, J. Li, J. Y. Liu and J. P. Xue, *J. Med. Chem.*, 2013, **56**, 5797–5805.
35 B. Zhao, W. Duan, P. C. Lo, L. Duan, C. Wu and D. K. P. Ng, *Chem.–Asian J.*, 2013, **8**, 55–59.
36 H. Li, F. R. Fronczek and M. G. H. Vicente, *Tetrahedron Lett.*, 2011, **52**, 6675–6678.
37 S. Tuncel, F. Dumoulin, J. Gailer, M. Sooriyaarachchi, D. Atilla, M. Durmuş, D. Bouchu, H. Savoie, R. W. Boyle and V. Ahsen, *Dalton Trans.*, 2011, **40**, 4067–4079.
38 A. Galstyan, K. Riehemann, M. Schäfers and A. Faust, *J. Mater. Chem. B*, 2016, **4**, 5683–5691.
39 S. G. Kimani, T. A. Shmigol, S. Hammond, J. B. Phillips, J. I. Bruce, A. J. MacRobert, M. V. Malakhov and J. P. Golding, *Photochem. Photobiol.*, 2013, **89**, 139–149.
40 J. Y. Liu, P. C. Lo, W. P. Fong and D. K. P. Ng, *Org. Biomol. Chem.*, 2009, **7**, 1583–1591.
41 C. F. Choi, J. D. Huang, P. C. Lo, W. P. Fong and D. K. P. Ng, *Org. Biomol. Chem.*, 2008, **6**, 2173–2181.
42 A. O. Ribeiro, J. P. C. Tomé, M. G. P. M. S. Neves, A. C. Tomé, J. A. S. Cavaleiro, Y. Iamamoto and T. Torres, *Tetrahedron Lett.*, 2006, **47**, 9177–9180.
43 E. Y. Xue, R. C. H. Wong, C. T. T. Wong, W.-P. Fong and D. K. P. Ng, *RSC Adv.*, 2019, **9**, 20652–20662.
44 L. Luan, W. Fang, W. Liu, M. Tian, Y. Ni, X. Chen and X. Yu, *Org. Biomol. Chem.*, 2016, **14**, 2985–2992.
45 E. Ranyuk, N. Cauchon, K. Klarskov, B. Guérin and J. E. van Lier, *J. Med. Chem.*, 2013, **56**, 1520–1534.
46 L. Li, Z. Luo, Z. Chen, J. Chen, S. Zhou, P. Xu, P. Hu, J. Wang, N. Chen, J. Huang and M. Huang, *Bioconjugate Chem.*, 2012, **23**, 2168–2172.
47 M. R. Ke, S. L. Yeung, W. P. Fong, D. K. P. Ng and P. C. Lo, *Chem.–Eur. J.*, 2012, **18**, 4225–4233.
48 M. Sibrian-Vazquez, J. Ortiz, I. V. Nesterova, F. Fernández-Lázaro, A. Sastre-Santos, S. A. Soper and M. G. H. Vicente, *Bioconjugate Chem.*, 2007, **18**, 410–420.
49 Ł. Lamch, J. Kulbacka, M. Dubińska-Magiera, J. Saczko and K. A. Wilk, *Photodiagn. Photodyn. Ther.*, 2019, **34**, 480–491.
50 Ł. Lamch, W. Tylus, M. Jewgiński, R. Latajka and K. A. Wilk, *J. Phys. Chem. B*, 2016, **120**, 12768–12780.
51 Ł. Lamch, J. Kulbacka, J. Pietkiewicz, J. Rossowska, M. Dubińska-Magiera, A. Choromańska and K. A. Wilk, *J. Photochem. Photobiol., B*, 2016, **160**, 185–197.
52 J. Cao, X. Gao, M. Cheng, X. Niu, X. Li, Y. Zhang, Y. Liu, W. Wang and Z. Yuan, *Nano Lett.*, 2019, **19**, 1665–1674.
53 W. Yu, M. Ye, J. Zhu, Y. Wang, C. Liang, J. Tang, H. Tao and Y. Shen, *Nanomedicine*, 2018, **14**, 1099–1110.
54 S. Wang, F. Yuan, K. Chen, G. Chen, K. Tu, H. Wang and L. Q. Wang, *Biomacromolecules*, 2015, **16**, 2693–2700.
55 M. N. Sibata, A. C. Tedesco and J. M. Marchetti, *Eur. J. Pharm. Sci.*, 2004, **23**, 131–138.
56 I. R. Calori, C. C. Jayme, L. T. Ueno, F. B. C. Machado and A. C. Tedesco, *Spectrochim. Acta, Part A*, 2019, **214**, 513–521.
57 C. Felip-León, O. Martínez-Arroyo, S. Díaz-Oltra, J. F. Miravet, N. Apostolova and F. Galindo, *Bioorg. Med. Chem. Lett.*, 2018, **28**, 869–874.
58 M. Obata, S. Tanaka, H. Mizukoshi, E. Ishihara, M. Takahashi and S. Hirohara, *J. Polym. Sci., Part A: Polym. Chem.*, 2018, **56**, 560–570.
59 N. Y. Borovkov, E. G. Odintsova, V. E. Petrenko and A. M. Kolker, *RSC Adv.*, 2019, **9**, 33969–33975.
60 M. Obata, S. Masuda, M. Takahashi, K. Yazaki and S. Hirohara, *Eur. Polym. J.*, 2021, **147**, 110325.
61 O. Shimokawa, H. Matsui, Y. Nagano, T. Kaneko, T. Shibahara, A. Nakahara, I. Hyodo, A. Yanaka, H. J. Majima, Y. Nakamura and Y. Matsuzaki, *In Vitro Cell. Dev. Biol.: Anim.*, 2008, **44**, 26–30.